Neuroinform (2012) 10:141–158
DOI 10.1007/s12021-011-9132-z

ORIGINAL ARTICLE

MEG-SIM: A Web Portal for Testing MEG Analysis Methods using Realistic Simulated and Empirical Data

C. J. Aine · L. Sanfratello · D. Ranken · E. Best · J. A. MacArthur · T. Wallace · K. Gilliam · C. H. Donahue · R. Montaño · J. E. Bryant · A. Scott · J. M. Stephen

Published online: 10 November 2011

Abstract MEG and EEG measure electrophysiological activity in the brain with exquisite temporal resolution. Because of this unique strength relative to noninvasive hemodynamic-based measures (fMRI, PET), the complementary nature of hemodynamic and electrophysiological techniques is becoming more widely recognized (e.g., Human Connectome Project). However, the available analysis methods for solving the inverse problem for MEG and EEG have not been compared and standardized to the extent that they have for fMRI/PET. A number of factors, including the non-uniqueness of the solution to the inverse problem for MEG/EEG, have led to multiple analysis techniques which have not been tested on consistent datasets, making direct comparisons of techniques challenging (or impossible). Since each of the methods is known to have their own set of strengths and weaknesses, it would be beneficial to quantify them. Toward this end, we are announcing the establishment of a website containing an extensive series of realistic simulated data for testing purposes (http://cobre.mrn.org/megsim/). Here, we present: 1) a brief overview of the basic types of inverse procedures; 2) the rationale and description of the testbed created; and 3) cases emphasizing functional connectivity (e.g., oscillatory activity) suitable for a wide assortment of analyses including independent component analysis (ICA), Granger Causality/Directed transfer function, and single-trial analysis.

Keywords MEG · EEG · Simulations · Database · Testbed · Inverse procedures · Connectivity · Visual Working Memory · Auditory · Somatosensory

C. J. Aine (✉) · L. Sanfratello · T. Wallace · C. H. Donahue · R. Montaño · J. E. Bryant
Department of Radiology, MSC10 5530,
University of New Mexico School of Medicine,
Albuquerque, NM 87131, USA
e-mail: aine@unm.edu

C. J. Aine · L. Sanfratello · E. Best · J. A. MacArthur · K. Gilliam · A. Scott · J. M. Stephen
The Mind Research Network,
Albuquerque, NM, USA

D. Ranken
Los Alamos National Laboratory,
Los Alamos, NM, USA

Introduction

There has been increased interest in the use of noninvasive functional imaging techniques for characterizing cognitive deficits in clinical populations. Furthermore, there has been renewed appreciation of the benefits for characterizing the fine temporal dynamics of these deficits. For example, one cannot learn about the direction of information flow through the brain, or information processing stages known to occur in various memory functions (e.g., identification, maintenance, recognition), without both excellent spatial and temporal resolution. Although magnetoencephalography (MEG) and electroencephalography (EEG) methods offer excellent temporal resolution, they face the greatest challenge to source localization of the neuroimaging techniques since the well-known "inverse problem" (i.e., the reconstruction of the current distribution inside the brain based on measurements made outside the head) is not as straightforward for MEG/EEG as it is for functional magnetic resonance imaging (fMRI) and positron emission tomography (PET) methods, due to the physics of the problem. The inverse problem for MEG and EEG is mathematically ill-posed; that is, it has no unique solution

in the most general, unconstrained case (Hämäläinen et al. 1993). Therefore, suitable constraints have to be applied to render the solution unique (Baillet et al. 2001).

For a number of reasons, discussed later, results from the varied inverse procedures have never been tested and compared using a standard testbed of realistic simulated data. It is standard practice in the MEG field to create computer-simulated data in order to test a newly developed or revised inverse procedure, using data where the ground truth (i.e., the solution) is known before testing it on empirical data where the ground truth cannot be known. Since each of the MEG analysis methods is known to have its own set of strengths and weaknesses [for some examples see (Liljestrom et al. 2005)], it would be beneficial to the community to qualify and quantify them. Therefore, we are announcing the establishment of a website containing a series of realistic simulated data for testing purposes (http://cobre.mrn.org/megsim/). If an algorithm provides reasonable solutions to simulations then it is standard practice to use the algorithms in simple sensory empirical data where the literature provides information on the expected locations and time-courses of sources (e.g., non-human primate studies) before attempting analysis of cognitive datasets where it is impossible to know the ground truth. Therefore, we acquired simple somatosensory, auditory, and visual sensory data on several participants for this purpose since it is best if the same empirical datasets are shared across the community for comparison. If an algorithm fails to identify the simulated sources and time-courses under realistic conditions (e.g., similar signal-to-noise ratio or SNR as empirical data and real artifacts occurring at random intervals), then one cannot expect to obtain correct or reasonable results in empirical data. The rationale and description of the testbed created along with sample simulated cases emphasizing functional connectivity and oscillatory activity are presented here. The single-trial datasets described are suitable for a wide assortment of analyses including independent component analysis (ICA), Granger Causality/Directed transfer function, and single-trial analysis.

Inverse Procedures For investigators new to this field, we briefly outline the most common inverse methods below. The source models and associated inverse algorithms fall into four broad categories. First, there are models that use a relatively low-order parametric description of the currents in order to produce an over-determined problem, i.e., the number of parameters to be estimated in the model is less than the number of recording sites. The most frequently used source model in MEG for clinical studies is a fixed set of equivalent current dipoles (ECDs) located at various cortical locations whose moments (ECD amplitudes) vary with time (Scherg and Von Cramon 1986; Mosher et al. 1992; Ermer et al. 2000). The term *equivalent* means that coherent activation of a large number of pyramidal cells can be represented by a point source at the detectors. Second, there are current reconstruction models that employ a grid of elementary sources in a volume or on the cortical surface such that the number of parameters to be estimated in the model is typically much greater than the number of measurements. Because the solution, in this case, is under-determined, the weighted least-squares criterion requiring that the prediction error is minimized, must be augmented with an additional constraint to select the "best" current distribution among those capable of explaining the data. In the case of the basic L2 minimum norm approach the mathematical criterion is the solution that minimizes the power (L2-norm) of the dipole moment (Wang et al. 1992; Dale and Sereno 1993; Hämäläinen and Ilmoniemi 1994; Ioannides et al. 1994; Pascual-Marqui et al. 1994; Grave de Peralta-Menendez and Gonzalez-Andino 1998; Uutela et al. 1999). The L1 minimum norm solution selects the source configuration that minimizes the absolute value of the source strength (Uutela et al. 1999; Huang et al. 2006). Third, there are spatial filter (e.g., beamformer) approaches that estimate activity at points or regions of interest, independent of one another. Beamformer output, for example, is a linear combination of the external field measurements at each time sample, constructed with the requirement that the focus is on the source of interest while minimizing contributions from all other sources (Van Veen et al. 1997; Vrba and Robinson 2000; Sekihara et al. 2001). That is, it allows signals of interest to pass through each volume grid node or cortical surface location while suppressing noise and signals from other locations (i.e., spatial filter). Finally, there are probabilistic approaches to the MEG/EEG source localization problem based on Bayesian inference [e.g., (Jun et al. 2005; Wipf et al. 2010)]. Some of these approaches result in a single best solution to the problem, while others use Markov Chain Monte Carlo to produce a large number of likely solutions that both fit the data and any prior information [e.g., (Schmidt et al. 1999)].

Limitations of Inverse Procedures Each of the inverse procedures has limitations associated with it. Critics of the earlier dipole modeling approaches emphasize the difficulties in: 1) accurately localizing more than one or a few point current dipoles; 2) using point current dipoles to localize extended sources; and 3) determining the number of sources to be included in the search *a priori* (Liu et al. 1998; Fuchs et al. 1999; Uutela et al. 1999; Huang et al. 2006; Lin et al. 2006; Mattout et al. 2006). Our greatest concern for the multidipole, spatiotemporal modeling methods is that under-estimation of the number of true sources can severely compromise location and time-course accuracy for the identified sources (Supek and Aine 1997;

Greenblatt et al. 2005). This is because multidipole modeling methods attempt to account for the entire measured signal via a given number of sources, and the omission of one source will generally change the position and/or magnitude of other sources to account for the signal from the omitted source. This is not true for the minimum norm, beamformer, or Bayesian methods. In contrast, critics of the minimum norm-based approaches state that: 1) the results often appear smeared, even for point current sources and at times may become split across lobes which produce spurious or ghost sources leading to imprecise estimated dynamics (David et al. 2002; Michel et al. 2004; Lin et al. 2006); 2) the constraints introduced are purely mathematical with no physiological justification (Michel et al. 2004); 3) the solution is biased toward superficial source locations leading to the application of depth weightings by some groups (Ioannides et al. 1990; Lin et al. 2006); 4) the smeared or broadened effect becomes more pronounced with a decrease in signal-to-noise, potentially leading to false positive sources (Wischmann et al. 1995); and 5) it is severely under-determined thereby requiring the use of regularization methods to restrict the range of possible solutions. Although, the linearly-constrained minimum variance (LCMV) beamformer has higher resolution than minimum norm-based methods when cortical sources are focal, the underlying assumption is that neural sources are incoherent. Coherent signals will cause the beamformer to fail in finding locations of other coherent sources due to partial cancellation (Hui et al. 2010) which is a potential problem for cognitive data where coherence typically abounds (i.e., working memory tasks). For example, in working memory studies, activity tends to synchronize across many widespread brain regions for seconds (Aine et al. 2003). However, several groups have recently introduced variants of the beamformer that can reportedly deal with coherent sources, with some restrictions [e.g., (Dalal et al. 2006; Brookes et al. 2007; Diwakar et al. 2011; Moiseev et al. 2011)]. Secondly, Hui and Leahy (2006; Hui et al. 2010) also noted that beamformers may not be appropriate, in their current form, for directly examining functional connectivity or cortical interactions, given the robust cross-talk present in the data. The latter is true for minimum norm-based methods as well. However, the general advantages of minimum norm and beamformer methods are that they require less analysis time making them quicker to use and the number of sources to be modeled does not need to be known *a priori*. Finally, less seems to be known about Bayesian methods since they have not been widely applied to real experiments (Luck 2005). In part this may be due to a need for large computational resources since some versions utilize a Markov Chain Monte Carlo approach to generate sets of activity parameters that are distributed according to the posterior distribution (Schmidt et al. 1999).

The simulated datasets described here are designed to provide a wide range of realistic examples which emulate brain activity. We specifically tried to design these simulations such that a particular approach would not always be favored. We hope developers will utilize these data to further develop and refine MEG analysis methods. Similarly, we hope that users of the algorithms will compare and contrast their favored approaches with others. Because we are avid users of a semi-automated, multidipole, spatiotemporal approach [Calibrated Start Spatio-Temporal or CSST; (Ranken et al. 2002, 2004)], solutions shown throughout this document are from the CSST algorithm, for immediate benchmark comparisons.

Barriers Addressed by Creating Realistic Simulated Datasets One barrier encountered in the area of software development for electromagnetic measures is the lack of an extensive, realistic simulated testbed for determining the success of the algorithms and for comparing algorithmic performance with others (i.e., standardization). Often developers test their algorithms using one or a few test cases that may or may not closely emulate real brain activity and often these test cases are not readily amenable for other developers to use. For example, white noise is often added to the data to simulate noise normally contained in data. The addition of real brain noise (e.g., ongoing background rhythms not related to the task) is more appropriate since real brain noise can have a dramatic effect on the localization ability of algorithms. Furthermore, users of algorithms would like to know how various analysis methods work in the modalities they are investigating (e.g., auditory, visual, somatosensory) or in the specific areas of their research interests (e.g., sensory or cognitive studies). Our realistic simulated datasets also show tremendous differences in SNR across participants for similar source locations, due to signal cancellation and summation associated with differences in cortical geometry [e.g., (Aine et al. 1996; Amunts et al. 2000; Stephen et al. 2003a, b)]. An algorithm may work well in one of the scenarios listed above but may be less than optimal in others. The creation of realistic datasets ranging from sensory to cognitive studies in auditory, somatosensory, and visual modalities and from a number of participants can help developers tremendously in understanding behaviors of their algorithms.

An additional barrier for MEG investigators is the fact that MEG systems made by different manufacturers have different pickup coils, sensor arrays, noise cancellation methods, as well as different software packages for data analysis. Many of the software implementations are specific to one particular data storage format or noise cancellation method as well. These factors make it extremely difficult to compare results or pool data across laboratories. If one

developer creates a simulated data set using the sensor geometry of the Elekta Neuromag 306 system, for example, then investigators using the VSM MedTech CTF 275 system usually cannot use it because of file formatting barriers. We have been working on software that is machine-independent (E. Best and D. Ranken) that can convert from one MEG system format to another. A standard testbed that can be used by all developers and users would be of great help to the MEG community, and hopefully to the EEG community in the future.

Structural and Functional Connectivity A current emphasis in neuroimaging is on structural and functional connectivity (e.g., the NIH Human Connectome Project) including the role oscillatory activity plays during cognition. Evidence now indicates that: 1) local field potentials, which provide a measure of mainly postsynaptic dendritic responses, show strong sub-threshold synchrony of ongoing fluctuations in the cell's membrane potentials (Lampl et al. 1999); 2) local networks are modulated by coordinated sub-threshold excitability changes (Engel et al. 2001); and 3) action potentials generated by cortical cells align with the oscillatory rhythm enabling neurons participating at the same oscillatory rhythm to synchronize their discharges with high precision across cortical regions (Gray et al. 1989). Although the specific roles these rhythmic activities play are still debated, numerous studies in monkeys and humans suggest that oscillatory activity plays an important role in integrating neural activity from distant cortical areas [e.g. (Jensen and Lisman 1998; Canolty et al. 2006; de Lange et al. 2008; Osipova et al. 2008)], such as prefrontal and parietal cortices (von Stein et al. 2000). Others add that these internally generated coherent fluctuations of excitability may also provide context to sensory information and predictions about forthcoming events (top-down processing) in order to guide behavior (Engel et al. 2001). Because of this increased interest in functional connectivity, we present cases of realistic simulations using both short- and long-range oscillatory activity (gamma and beta band) and cases where activity is correlated during later intervals (e.g., simulating working memory).

Methods and Results

Simulated data were created using MRIVIEW and MEGAN software. A brief description of these tools is provided below. MRIVIEW (Ranken and George 1993; Ranken et al. 2002) is a software tool (http://cobre.mrn.org/megsim/tools/mriview/mriview.shtml) for integrating volumetric MRI head data with functional information (e.g., EEG, MEG, fMRI). It provides tools for visualizing MRI data in a variety of 2D and 3D formats, the latter of which is an object-based environment that is used to combine structural MRI data with various representations of brain functional data. A Coordinate Transformation interface allows users to quickly perform MEG/EEG to MRI transformations, needed for both showing MEG/EEG results on MRI based anatomy, and for setting up MEG/EEG forward models.

A Segmentation Interface module provides automatic and manual segmentation procedures to support a variety of segmentation tasks, including: variable resolution grid creation for CSST, gray/white matter segmentation, extraction of 3-layer surface models for BEM analyses, and 5 (or more) tissue-type classifications for Finite Element Models (FEM) or Finite Difference Head Models (FDM). A Forward Simulator is included for creating multiple MEG and/or EEG focal or distributed-source regions of arbitrary size and orientation for testing various inverse procedures (see Fig. 1A). User-specified, ellipsoid regions of gray/white matter boundary can be labeled and used to create simulated regions of activity. We have used these tools previously for simulating epileptic spikes that were then embedded in spontaneous activity from each subject (Stephen et al. 2003a, 2005). In the example shown in Fig. 1A, a Freesurfer-segmented gray matter/white matter boundary for the simulations (shown in red) was imported into MRIVIEW. The EEG forward solution uses the Sun algorithm (1997) and the MEG forward solution uses the Sarvas formula (1987). The simulated activation time-courses can be generated using multiple Gaussians or a sinusoid (Fig. 1B), or they can be read from a file. Sensor geometries used by the major manufacturers of MEG whole-head arrays (e.g., Elekta Neuromag Ltd, VSM MedTech CTF Systems, 4-D Neuroimaging) for generating the forward fields are obtained from a sister software package, MEGAN (E. Best), which organizes the data from the different MEG systems into a consistent data format, netMEG, a self-documenting and highly portable file, written using netCDF format. The simulated sensor measurements are obtained by summing the forward fields from all of the simulated sources. Either simulated noise or real noise from MEG/EEG acquisitions (Fig. 1C) can be added to the calculated forwards to generate better simulations of empirical MEG/EEG data (Fig. 1D). MEGAN, http://cobre.mrn.org/megsim/tools/MEGAN, is also written in IDL and allows one to conduct preliminary analyses on data from different MEG systems such as deletion of bad channels, digital filtering and artifact rejection for retrospective averaging relative to a stimulus or response record, visualization of a variety of forms (e.g., static field distributions, temporal waveform displays and movie formats), and temporal analysis. The netMEG output file format can be used by CSST, constrained linear inverse procedures, and Bayesian Inference analysis.

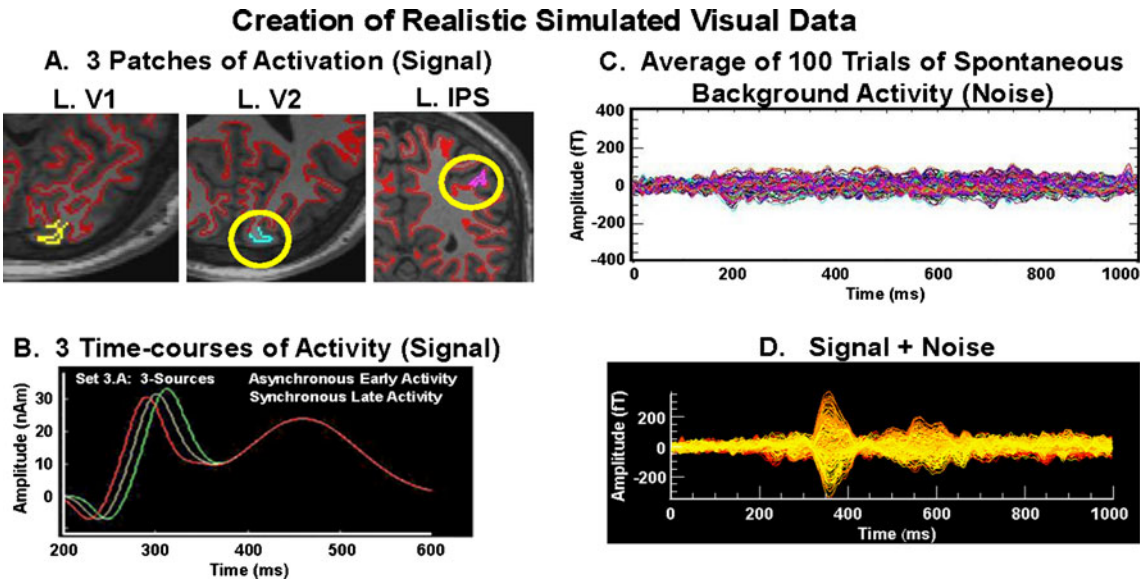

Fig. 1 A Freesurfer-segmented gray matter/white matter boundary for the simulations (shown in red) was imported into MRIVIEW from which patches (**A**) of simulated activity (**B**) were generated. 100 passes of spontaneous activity or noise (**C**) were identified using CTF software (Data Editor) and averaged together using MEGAN. The simulated activity was embedded within the averaged noise file (**D**) and saved in netCDF format (i.e., a netMEG file in MEGAN)

CSST (Calibrated Start Spatio-Temporal) Analysis This multi-dipole, spatio-temporal approach has been automated, i.e., it takes the traditional starting parameter guesses out of the hands of the investigator. CSST uses the Nelder-Mead non-linear downhill simplex procedure to perform a spatial search (Nelder and Mead 1965) and utilizes information based on a singular value decomposition (SVD) of the data matrix for determining a range of number of sources to be localized. Advantages of the newer CSST automated algorithm, compared to MSST (Multi-Start Spatio-Temporal) (Harrison et al. 1996; Huang et al. 1998; Aine et al. 2000), lie in the fact that more fits to the data can be accomplished in less time, while still employing a reduced chi-square statistic as the cost function for obtaining the best fits to the data. CSST runs multiple instances of a downhill simplex search from random combinations of MR-derived starting locations from within the head volume, on a Linux PC cluster. General steps for processing the MEG and MRI data are shown in Fig. 2. A two stage simplex procedure is used to first rule out sub-optimal solutions (i.e., it utilizes a coarse convergence criterion in the simplex procedure), and then to refine the remaining solutions using a fine convergence setting. A parallel version of CSST is currently running on the Linux clusters at the Mind Research Network (MRN), using MPI to distribute the calculations across the processors, which could eventually provide real-time, multi-dipole MEG analysis through the use of Graphics Processing Units on multicore personal processors. CSST has been used extensively with both Neuromag 122 and CTF 275 MEG systems (Stephen et al. 2003a, b, 2005, 2006; Aine et al. 2010). CSST has also been used to analyze Neuromag Vectorview 306-channel data and has been thoroughly tested on EEG data (Susac et al. 2010, 2011; Golubic et al. 2011). Additional information on our analysis methods can be found in Aine et al. 2010. Sphere and overlapping-spheres forward models are options within MRIVIEW (Huang et al. 1999) but a Forward Interpolation capability (Ermer et al. 2001) has also been implemented in CSST, allowing it to be used with BEM or FEM/FDM forward models. CSST accuracy tests were performed on CTF 275 data obtained from a dry-phantom current dipole generator, demonstrating 1 mm dipole source localization accuracy.

Simulated Datasets

Empirical MEG/MRI datasets have been acquired for 5 participants under a partnership formed between the MRN, Massachusetts General Hospital, University of Minnesota/Veterans Affairs in Minneapolis, University of New Mexico, and Los Alamos National Laboratory. Data were acquired using 3 different MEG systems (VSM MedTech 275, Elekta-Neuromag 306, 4-D Neuroimaging 3600) and 3 different sensory paradigms (visual, auditory and somato-sensory) for each participant. These empirical data will be made available via the MEG-SIM portal and will be discussed more completely later. A grant from NIMH (R21MH080141) allowed us to then create realistic

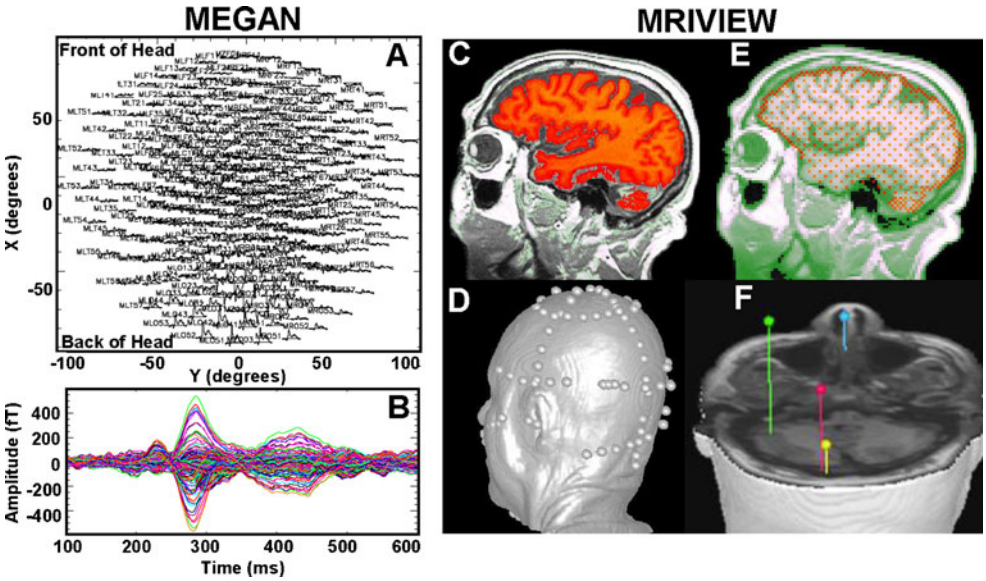

Fig. 2 MEGAN is used for preprocessing the MEG data. These data are saved in netCDF format and used as input for the CSST algorithm. (**A**) averaged simulated visual responses (Sim 1.B) - whole head array; (**B**) averaged simulated visual responses for each sensor are overlaid (200–600 ms interval was analyzed). MRIVIEW was used for: 1) segmenting the cortical volume (**C**); 2) conducting a least squares fit between the points digitized on the head surface and the reconstructed MR surface (**D**); 3) determining the starting locations (red dots) and best-fitting sphere head model (**E**); and 4) setting-up the CSST fits and displaying the CSST source localization results (**F**). Multistart algorithms analyze thousands of fits to the data, as opposed to a single fit, enhancing the probability of reaching the global minimum and obtaining statistically adequate and accurate solutions (e.g., 15,000 fits to the data were conducted for this 4-dipole model). Adapted from Fig. 1, Neuroimage, 49(4): 3319–3330, 2010, with permission from Elsevier

simulated data derived from the real noise contained in the collected data and to establish a web portal for others to access these simulated datasets. We refer to the testbed as 'realistic' simulated data because: 1) colored noise is used in most examples (i.e., spontaneous data containing correlated noise); 2) the time-courses and source locations simulated are based on findings from empirical data; 3) different-sized cortical patches are created from MRIs of individual participants (i.e., the SNR and orientation of sources differ across participants); and 4) in some cases each of the unique single trials, mimicking actual data acquisition, are provided.

Focal vs. Extended Sources Examining source extent in the simulated and empirical studies is important for evaluating the suggestion that ECD modeling is limited due to its proposed inability to deal effectively with extended sources (Dale et al. 2000; Hillebrand and Barnes 2002; Lin et al. 2006; Ahlfors et al. 2010; Golubic et al. 2011). The simulated datasets were constructed using two different-sized patches of cortex determined via MRI (~4 mm^2 and ~20 mm^2) producing two different source strengths (30 and 50 nAm). We used these values because: 1) our previous empirical results suggest that those current strengths are typical of what is encountered in sensory studies [e.g., Fig. 3 and Table 2 in (Aine et al. 2006) and Fig. 4 and Table 3 in (Aine et al. 2005) show similar peak amplitudes for visual and auditory studies] and 2) the sensory visual paradigm used to acquire data at each MRN partner site utilized small and large stimuli (1.0° and 5.0° of visual angle) designed to activate ~4 mm^2 of tissue and ~20 mm^2 of tissue in primary visual cortex, according to the cortical magnification factors presented in Rovamo and Virsu (1979). We attempted to equate the simulated and empirical parameters since the goal was to produce both focal and extended activity. The somatosensory study used electrical stimulation of the median nerve and the index finger, in order to produce focal vs. extended sources. The auditory study used 3 pure tones and bursts of white noise to evoke focal vs. extended activity.

Physiologically Plausible Time-courses Figure 3 shows sample time-courses from both a monkey and a human (left and right columns) in response to Walsh stimuli (visual). This spike-like activity followed by a slow sustained response is quite common for sensory and cognitive studies. Recent monkey studies suggest that the initial feedforward flow of information (i.e., the spike-like activity) establishes the neuron's classical receptive field and its basic tuning properties typically associated with *pre-attentive* processes (within 100 ms) (Lamme and Roelfsema 2000). Visual cortical neurons remain active after their participation in the feedforward sweep which allows information from horizontal and feedback connections to be incorporated into the response (i.e., the slow sustained response); massive feedback projections carry information from higher-order regions to forward

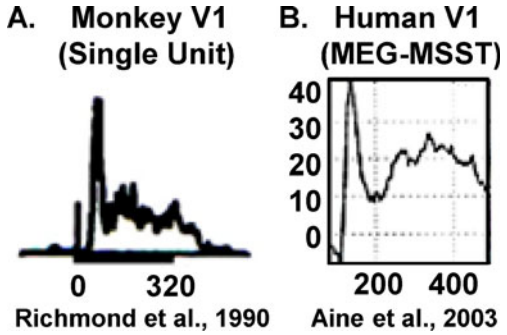

Fig. 3 (**A**) Single unit activity from monkey area V1 evoked by a Walsh function visual stimulus. (**B**) MSST human time-course from area V1 evoked by a Walsh function stimulus

projecting pyramidal cells of lower-order areas (Cauller 1998). Attention and memory processes influence lower-level responses via these horizontal and feedback connections which affects the late sustained activity following the initial burst (Lamme and Roelfsema 2000; Mehta et al. 2000; Bisley et al. 2004). This type of response profile is evident in many MEG visual and auditory studies (Portin et al. 1999; Aine et al. 2003, 2005; Vanni et al. 2004; Kovacevic et al. 2005) and were therefore modeled in the simulated data for physiological reality.

Simulated Visual Data Nine simulated visual datasets (1-sec epochs including equal pre- and poststimulus intervals) were generated consisting of a range of source configurations from simple to complex using small and large cortical patches. The locations and timing of the 3–7 simulated sources (see Table 1) were generated based on our previous basic visual (Stephen et al. 2002) and visual working memory studies (Aine et al. 2006). For example, time-courses associated with each cortical source in visual cortex were delayed by 10 ms, as shown in Table 1 in (Stephen et al. 2002). We varied the synchronicity of the latter portion of the time-courses across sets in order to determine an algorithm's sensitivity to fine temporal changes. Parameters that vary within and across datasets include: number of sources, focal vs. extended sources, current strengths, and degree of synchronicity of sources and noise level or type of noise (white noise or spontaneous noise). These 7 sets are being produced for 5 participants which result in datasets derived from different cortical geometries and different SNRs. In addition, they are being produced using CTF Omega 275, Vectorview 306, and Magnes 248 configurations. In each case, 100 single trials of real spontaneous background activity were averaged as a noise trial for each of 5 participants and for each of 3 MEG systems. At present, a spherical head model was used for the simulations and modeled data; however, a boundary element model (BEM) is available for future EEG and MEG simulations.

Visual Source Locations, Timing and Strengths The following visual areas were approximated on the cortical surface of the participants; V1, V2/V3, inferior lateral occipital gyrus (I.LOG), and intraparietal sulcus (IPS) (Stephen et al. 2002; Aine et al. 2006). To simulate a cognitive dataset three additional cortical regions were added, dorsolateral prefrontal cortex (DLPFC), right hippocampus (RH), and anterior cingulate (AC) since they have been shown to be responsive to visual working memory tasks (Aine et al. 2003, 2006; Nyberg et al. 2003) and they provide a good test for localizing deeper sources.

Visual Dataset 1 (A-B) This set represents the simplest case where all 3 sources are asynchronous (10 ms delays in onset times). In Set 1A all sources are small cortical patches (4 mm^2, 30 nAm) while in Set 1B all sources are large cortical patches (20 mm^2, 50 nAm). See Fig. 4 (top row).

Table 1 Onset latencies and amplitudes of sources in different visual areas used for each simulated dataset. Note that Set 3 differs from Set 1 in having synchronous late activity. Set 1.B and 3.B differ from 1.A and 3.A in dipole strengths (i.e., larger cortical patches). Note, these latencies are modeled after empirical visual studies but they were embedded in the noise file so that ~200 ms was effectively treated as prestimulus baseline with ~200 ms post-stimulus (i.e., the activity was centered in the noise files). *DLPFC and AC were treated as ramping activity peaking later in time

	V1	V2/V3	I. LOG	IPS	S. LOG	DLPFC	AC	RHC
Set 1.A	80 ms	90 ms		100 ms				
	30 nAm	30 nAm		30 nAm				
1.B	80 ms	90 ms		100 ms				
	50 nAm	50 nAm		50 nAm				
Set 2		90 ms	90 ms	100 ms				
		15 nAm	30 nAm	30 nAm				
Set 3.A	80 ms	90 ms		100 ms				
	30 nAm	30 nAm		30 nAm				
3.B	80 ms	90 ms		100 ms				
	50 nAm	50 nAm		50 nAm				
Set 4		90 ms	90 ms	100 ms	100 ms	300 ms*	400 ms*	
		15 nAm	30 nAm	20 nAm	30 nAm	20 nAm	30 nAm	
Set 5		90 ms	90 ms	100 ms	100 ms	300 ms*	400 ms*	80 ms
		15 nAm	30 nAm	20 nAm	30 nAm	20 nAm	30 nAm	51 nAm

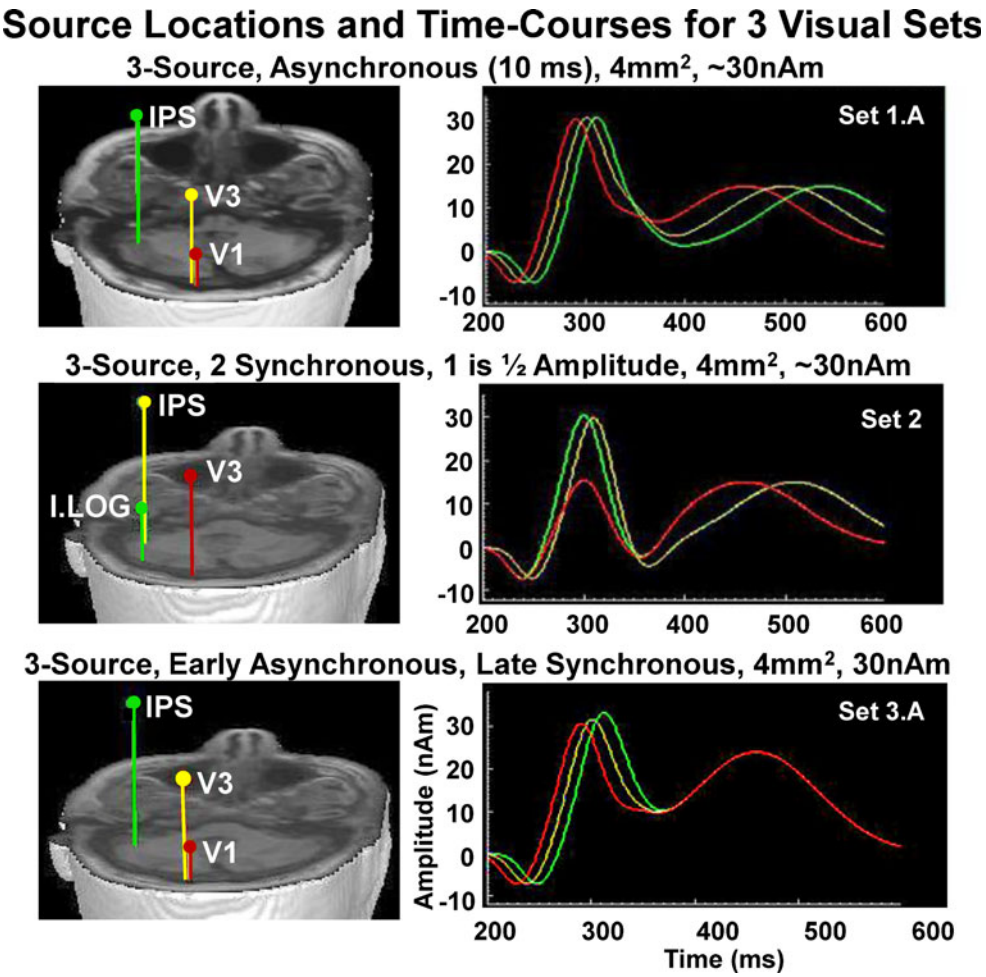

Fig. 4 Sample source locations and time-courses for 3 of the simulated cases. Note the subtle differences in temporal dynamics between these test cases

Visual Dataset 2 Two synchronous sources with one source half the intensity of the other (30 and 15 nAm), overlapped with an asynchronous source (onsetting 10 ms later and 30 nAm strength) are modeled in this set (see Fig. 4 middle row). This source configuration has been used by us extensively in the past since it provides a good test for resolving synchronous activity (Supek and Aine 1997; Huang et al. 1998), but the present implementation is more realistic in terms of the shapes of the time-courses and use of real noise. Note, binaural stimulation also activates coherent sources of activity; only the sources are not as closely spaced (i.e., left and right Heschl's gyrus).

Visual Dataset 3 (A-B) This set contains initial asynchronous activity (same as Set 1 A–B) from 3 sources which become synchronous later in time (Fig. 4 bottom row). There has been recent interest in using MEG to identify large-scale interactions between brain regions in cognitive tasks (neural networks) (David et al. 2002; Aine et al. 2003); synchronous late activity is often witnessed in these types of tasks. As noted by David et al. (2002) some inverse procedures are not designed to localize coherent sources (e.g., some LCMV beamformer approaches). Our visual working memory studies usually reveal late synchronous activity (Aine et al. 2003, 2006).

Visual Datasets 4–6 In Set 4, six sources of activity are modeled where one pair of sources is synchronous (one small and one large cortical patch with consequent differences in intensity). This type of profile builds off of Set 3 by making it more consistent with our working memory studies where initial asynchronous activity is followed by late activity in several disparate brain regions (including dorsolateral prefrontal cortex, anterior cingulate and superior lateral occipital gyrus) that become synchronous over time (Aine et al. 2003). Singer (1999), along with many others, suggests that synchronous neuronal firing provides one mechanism for binding the different features/attributes of stimuli across widespread cortical areas. Table 2 shows actual source locations, CSST estimated source locations, and errors when either noise was absent (no-noise) or real noise was present. Average error across the 6 sources was 0.1 mm for the no-noise condition and 6.8 mm for the real noise condition. This

Table 2 Actual and CSST estimated ("no-noise" and "real-noise") locations for a 6-source, realistic simulation. CTF head-centered coordinate system is utilized where –x points out the back of the head, +y points out the left ear and +z points out the top of the head. Standard deviation (SDev) is shown for estimated solutions for real-noise simulated data

SET 4 6 sources	Source V3			Error (mm)	Source I. LOG			Error (mm)	Source IPS			Error
	X	Y	Z		X	Y	Z		X	Y	Z	
Actual	−70.0	5.9	75.8		−59.7	33.2	42.9		−22.1	38.3	82.6	
No noise	−69.7	6.0	75.9	0.3	−59.8	33.3	42.9	0.1	−22.1	38.2	82.7	0.1
Real noise	−61.3	4.3	74.1	9.0	−55.6	31.7	44.5	4.6	−18.7	28.7	71.8	14.8
SDev (Real)	0.3	2.3	1.6		1.6	0.3	0.4		1.5	1.7	0.9	
	Source R. Frontal				Source AC				Source S. LOG			
	X	Y	Z		X	Y	Z		X	Y	Z	
Actual	58.1	−41.5	46.2		74.1	−7.0	47.8		−31.3	−40.7	60.3	
No noise	58.1	−41.7	46.2	0.1	74.0	−7.1	47.6	0.2	−31.4	−40.8	60.3	0.1
Real noise	58.5	−43.2	44.0	2.8	72.6	−9.9	46.7	3.4	−27.5	−36.1	59.1	6.1
SDev (Real)	0.1	0.1	0.4		0.5	0.3	0.2		0.5	0.6	0.6	

table demonstrates that the presence of real noise does significantly affect source localization accuracy; however, our CSST solution for the real noise condition was still good for this complicated dataset and inconsistent with previous critiques of dipole modeling approaches that state dipole methods cannot accurately localize more than a few point sources of activity.

Set 5 is the same as Set 4 with the addition of a source in right hippocampus (7 sources of activity). Set 6 (not shown in Table 1) is a case where late activity (e.g., 400–600 ms) was synchronous across four cortical sites (V1, I. LOG, IPS, and DLPFC), also seen in working memory studies. The upper left panel of Fig. 5 displays the locations of the cortical patches (cortical patches are located at the cross-hairs) while the time-courses assigned to the cortical patches are shown beneath the MRIs. The averaged waveforms (128 trials with signals embedded in real spontaneous noise) seen across 275 channels are shown in the middle left column. CSST source locations are shown in the upper right panel (see tabled values). The table shows the coordinates of the actual sources, the estimated source locations, and the errors using Euclidean distance. Net source orientation errors were 42.0° for V1, 58.2° for I. LOG, 20.9° for IPS and 48.0° for the DLPF sources. The middle right panel shows the estimated time-courses and source locations. The average error across all 4 sources was 6.7 mm with the greatest error for the I. LOG source. The cross-correlations between time-courses are shown in the bottom row of this figure. We examined early activity first (200–350 ms–bottom left panel) which shows that V1 activity correlated highly with I. LOG (dark blue tracing), regions showing the initial spike-like activity (~280 ms). IPS and DLPF cross-correlations were also highly correlated and near the zero-lag (orange tracing). The maximal correlation coefficients of the other pairs of sources were lower in value and were not near the zero-lag. In contrast, the late activity (350–600 ms—bottom right panel) shows higher zero-lag correlation coefficients for activity between the 4 brain regions (i.e., late activity was synchronous across brain regions) with IPS and DLPFC revealing the highest correlation coefficient (orange tracing). These data are also suitable for examining basic coherence between sensors.

Single-trial and Oscillatory Datasets (Sets 7–9) Single-trial datasets reflecting functional connectivity in a working memory task were created with and without oscillatory activity and are suitable for most types of analyses (i.e., ICA, time-frequency analysis, Granger Causality, etc.). In each case, sources embedded within 128 single trials of noise were jittered about their mean latency and amplitude. Set 7 is similar to Set 6 (VSM-CTF MEG System) only now each of the 128 single trials is available. Again, the four cortical sites were: 1) primary visual cortex (V1); 2) inferior lateral occipital gyrus (I.LOG); 3) intraparietal sulcus (IPS); and 4) dorsolateral prefrontal cortex (DLPFC). The cortical patch current strengths were initially assigned values similar to those we observe in our visual working memory studies (30–50 nAm peaks) using the MRIVIEW Forward Simulator (Ranken and George 1993; Ranken et al. 2002) and were then randomly jittered about those values by up to +/− 50% across the single trials. Peak latencies were also jittered across each trial by a randomly selected value up to +/− the full width at half maximum (FWHM) divided by 2. To allow for traditional source analysis of averaged evoked responses, the 128 single trials were then averaged together and written out to the netCDF file format.

In Set 8, oscillatory activity was added to Set 7 time-courses (Fig. 6). For the time-locked oscillatory activity,

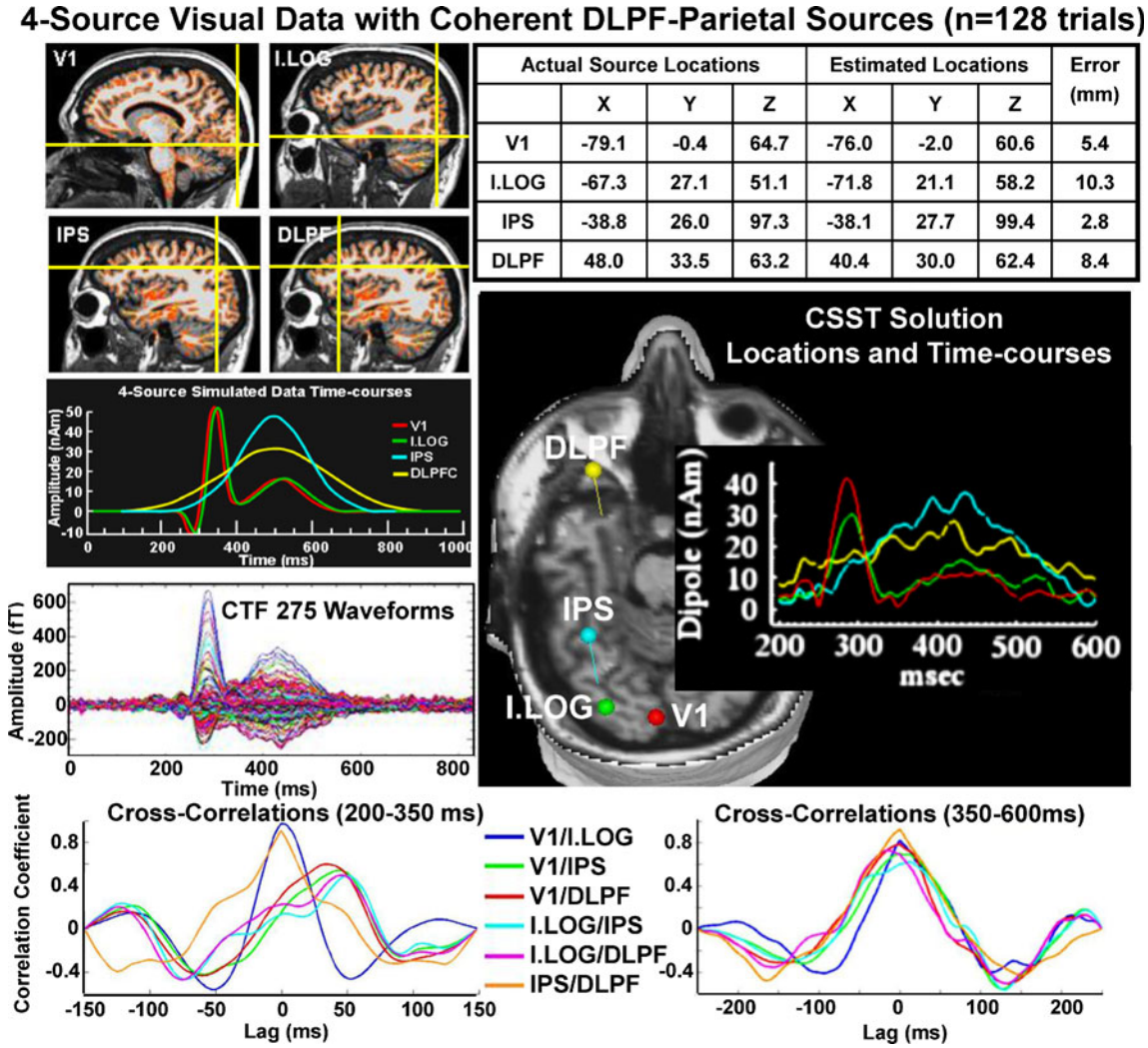

Fig. 5 Simulation results for a 4-source model where all sources became synchronous during the later interval (see upper left panels for source locations (cross-hairs) and time-courses of the sources). Amplitudes and peak latencies were jittered across each of 128 single trials. The averaged waveforms seen at the sensor level for the CTF system are shown beneath the input time-courses. Upper right table shows CSST actual locations and errors associated with modeled source locations. The middle panel shows location and time-course plots of the CSST solutions. Bottom row shows cross-correlations between source time-courses for an early interval (*left*) when there was some asynchrony across sources and a later interval (*right*) when all sources became synchronous. Adapted from Fig. 3, Brain Topography, 24:323–339, 2011, with permission from Springer

V1, I. LOG, and IPS oscillated between 30 and 60 Hz (gamma band) across the 128 trials while IPS and DLPFC oscillated between 14 and 28 Hz (beta band). Oscillatory activity for DLPFC was delayed by 20 ms relative to IPS and IPS gamma activity was delayed by 10 ms relative to IPS beta activity (see schematic in Fig. 6A). The delays were meant to reflect normal time delays between visual areas (Stephen et al. 2003a, b). Gamma activity mimicked local circuitry activity between V1, I. LOG, and IPS while beta activity mimicked long-range connections between IPS and DLPFC. For both beta and gamma oscillations, the amplitudes were set at 10 nAm and were then jittered between 5 and 15 nAm across the 128 trials. Note that the latencies, and therefore the phase of the oscillations, were kept constant between brain regions, and also between trials. As with the first simulated data set, the time-courses were constructed within MRIVIEW, however, they had to be constructed independently; i.e., one time-course contained the evoked response plus real noise while the other time-course contained the oscillations without noise. The two time-courses were then added together using Matlab. Again, to allow for source analysis of the averaged responses, the 128 single trials were averaged together to create a single averaged trial, and were then written out to a netCDF file. Datasets for two subjects were created this way.

Figure 6B shows the input signal at the sensor level across sources before oscillatory activity was added. Sample single-trials are shown where peak amplitudes (of both the evoked

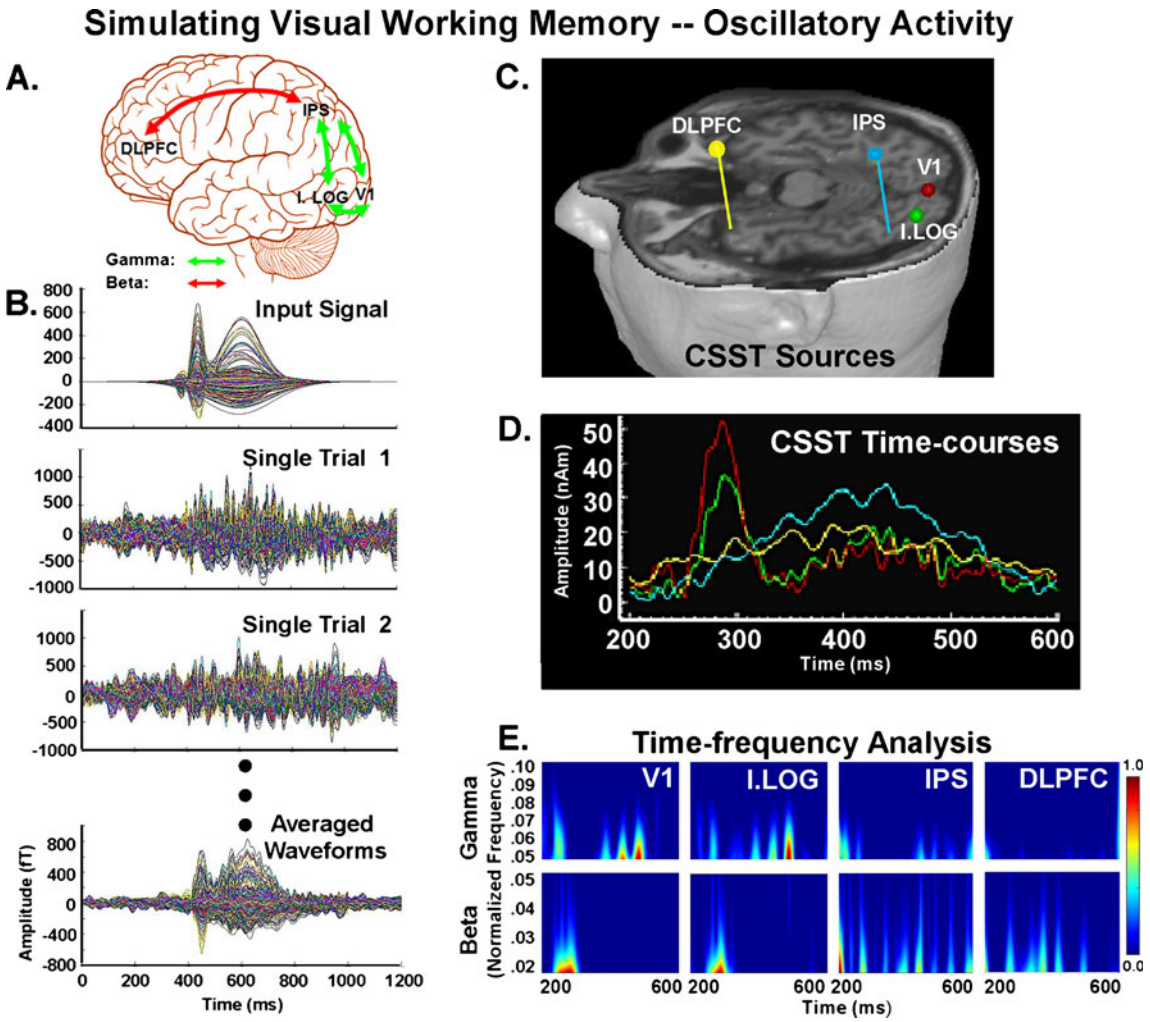

Fig. 6 Simulated visual working memory study with long-range beta band and short-range gamma band oscillatory activity (see (**A**) schematic). DLPFC and IPS oscillated at 15–20 Hz while IPS, I. LOG, and V1 oscillated at 30–80 Hz. IPS generated both beta and gamma band oscillations. (**B**) The averaged input signal without noise is shown followed by sample single-trials and the averaged data as seen at the sensors of the CTF system. (**C**) CSST location estimates and their associated time-courses (**D**) are shown. (**E**) Time-frequency representations using Morlet wavelets for the CSST solutions shown above. Frequency was normalized to the Nyquist frequency=½* sampling frequency (600 Hz). Oscillatory activity was given 10 nAm on average across trials, which is fairly weak activity

and oscillatory activity), peak latencies (of the evoked activity only), and frequency of the oscillatory activity were jittered across trials so each single trial is unique. Finally, the average of the 128 single trials is shown beneath. Figure 6C and D shows the output of the CSST algorithm. CSST provides both the locations of the dipoles and the reconstructed time-courses of activity. Table 3 contains the results of this analysis for the two visual/working memory datasets that were created for the first subject (i.e., single trials averaged with and without oscillatory activity). Our results show that CSST accurately reconstructs both temporal and spatial characteristics of the simulated datasets, even with noisy and oscillating sources. Time-frequency plots are shown in Fig. 6E for gamma and beta bands. Gamma band activity is primarily seen in dipoles located in V1, I.LOG and IPS, which is consistent with the simulated data. No gamma activity was provided to DLPFC and correspondingly, gamma activity during this interval of time is essentially non-existent. It appears that the initial spike-like activity in the time-course has a predominantly beta component to it as seen in the V1 and I.LOG beta band plots. IPS and DLPFC, in contrast, reveal beta band activity throughout the interval, which is consistent with the simulated data. Our realistic simulated oscillatory activity will provide a very nice dataset for testing various frequency analyses and inverse procedures. Again, these data also come with all 128 unique individual trials for investigators wishing to try single trial analysis methods.

For the final simulated dataset (Set 9), the same data as Set 8 was created with the difference that the noise trials and sensor configuration were taken from the empirical resting data acquired using the Neuromag 306 system. In this case, a Matlab program utilized the netCDF toolbox for

Table 3 CSST results for 4 visual sources based on averaged waveforms without oscillatory activity (top section) and with oscillatory activity (bottom section) for subject #1 (M545)

	CTF Subj. M545		
Source	Loc. Error (mm)	Lat. Error (ms)	Amp. Error (nAm)
Single trials (Set 7):			
V1	1.5	6	2.5
I.LOG	9.4	4	3.2
IPS	3.7	3	7.9
DLPF	8.9	13	6.8
Single trials with oscillations (Set 8):			
V1	4.7	6	9.8
I.LOG	9.7	1	4.8
IPS	7.0	1	11.2
DLPF	4.9	16	2.4

manipulating the opening and closing of the netCDF files containing the individual evoked waveforms and the individual oscillatory waveforms, which were created at cortical locations similar to Set 7. The simulated data were again created using MRIVIEW and MEGAN. Matlab was used to import the time-courses of the individual areas of evoked activity which were then jittered (in the same way as discussed above) and combined with randomly selected instances of Neuromag 306 noise which was read into Matlab using Fieldtrip functions (http://fieldtrip.fcdonders.nl/). One hundred single trials were created in this way, containing evoked and oscillatory activity from DLPFC, V1, IPS, and ILOG. This was, therefore, an automation of what was initially done with the previous single-trial data, Set 8. The 100 single trials were then averaged together and saved to a netCDF file, to be used with CSST analyses, and to a Neuromag 306 system fif file to be used with Curry, a commercial software package (Compumedics Neuroscan, Charlotte, NC http://www.neuroscan.com/) for sLORETA and SWARM analyses (Wagner et al. 2007). This is just one example of the different versions of single-trial simulations that can be created and which will be placed on the MEG-SIM website. Others to be included can have a variety of intra- and inter-trial variability, and/or can be created for different brain regions altogether. As additional examples, we have created simulations with: 1) random jitter across sources within-trials for both induced oscillatory and evoked activity; 2) constant phase across sources within-trial but jittered across trials for both induced and evoked activity; and 3) constant phase lag between two oscillating brain sources with a third source that has a random phase lag, in reference to the other two active areas, in each trial. We have also created simulations in continuous fif format with triggers indicating where the activity begins. This last example will be especially useful for software packages that cannot read in single trial simulations.

Multidipole, spatiotemporal source localization was conducted for subject #2 (M072) using the CSST algorithm for simulated data Sets 8 and 9 (CTF and Neuromag systems, respectively). Table 4 shows the results from these analyses. Once again CSST determines the locations of the active cortical areas with a good degree of accuracy. We do find obvious differences between the results for the CSST dipole fits for the two different subjects. This was not surprising since the simulations were 1) created using each subjects' MRI, therefore, the exact location of the cortical patch differs somewhat between subjects which will result in different waveform distributions at the sensor level for the different MEG systems; and 2) the V1 source was given a smaller initial amplitude (30 nAm versus 50 nAm) in subject #2 (M072), making it more difficult to identify. Furthermore, there is also a slight variation in how accurately each source is located depending on the MEG system used to collect the empirical data from which the noise trials were taken to create the simulated data.

We next report the results of two L2 minimum norm-based current distribution analyses, sLORETA and SWARM, available in Curry for the datasets made for subject #2 (M072). In current distribution models, the cortex is divided up into a large number of elements, which form the solution space. Since the primary source of the MEG signal is assumed to be associated with postsynaptic currents, a current dipole is assigned to each of the many tens of thousands of tessellation elements. Additionally, since the problem is under-determined (i.e. there are fewer equations than unknowns), the weighted least-squares criterion requiring that the prediction error is minimized must be augmented with an additional constraint to select the best current distribution among those capable of explaining the data. In the case of the basic L2 minimum norm approach, the mathematical criterion is the solution that minimizes the power (L2-norm) of the dipole moment. After adding noise normalization, statistical significance of current estimates relative to the level of noise can be determined using "dynamic statistical parametric" maps; sLORETA is a

Table 4 CSST results for subject #2 (M072) for both CTF and Neuromag systems. Location was considered "not found" if it was ≥50.0 mm from the true source

Source	CTF M072	Neuromag M072
Single trials & oscillations:	Loc. Error (mm)	Loc. Error (mm)
V1	not found	9.9
I.LOG	7.5	3.7
IPS	4.2	2.8
DLPF	2.1	4.7

variation of this approach (Pascual-Marqui et al. 1994, 1999; Dale et al. 2000; Pascual-Marqui 2002; Wagner et al. 2004, 2008), while SWARM (Wagner et al. 2007, 2008) is an sLORETA-based method that provides current estimates instead of probabilities. Simulated data was read into the Curry software package using either .ds files (for the CTF simulations) or .fif files (for the Neuromag simulations). This allowed Curry to identify the correct coordinate system to use when importing the data and additionally allowed digitized fiducials in the files to be used for accurate alignment with the subjects MRI, which was also imported into Curry.

Figure 7 shows the results of the sLORETA and SWARM analyses carried out using the Curry software package. The simulations made using the CTF system show results that are more distributed in the IPS/I.LOG/V1 areas in both sLORETA and SWARM in comparison to the simulations made with the Neuromag system, which shows more focal solutions. This is not particularly surprising based on the fact that planar gradiometers are more sensitive to signals directly below the sensors. We additionally provide the results at two different cutoffs, to show that some activation may not be seen if the cutoff is too high, e.g. compare the CTF sLORETA results in Fig. 7, where the DLPFC area of activity is lost at the higher cutoff. Figure 7 also shows that sLORETA was unable to find DLPFC activity at either cutoff in the Neuromag data. It is also possible to extract time-course activation from the SWARM analysis. Although Curry software provides time-course extraction via "CDR dipoles" it also contains the functionality to save the SWARM results into a mat file, which may then be read into Matlab for further investigation. We utilized the latter method. As a first step to show how time-courses can be extracted from the SWARM data we chose to identify areas of activation as simply as possible. To this end we had Matlab identify the areas of highest activation from the SWARM data that Curry created and plot the time-courses at those locations (right portion of Fig. 7), the only constraint was that the independent sources be greater than 2.0 cm apart. Note that the added oscillations can be easily identified. We have less experience with the two L2 minimum norm-based analyses, therefore they should be considered preliminary at best; consequently, no tables of error values are offered. We present a preliminary report here hoping to encourage others to investigate these areas further using these data. It is clear that these simulated datasets are already providing a reasonable challenge for a variety of analysis methods, which is our goal.

Somatosensory and Auditory Datasets Simulating median nerve stimulation (Fig. 8) provides one of the simplest cases. This activity consists of contralateral primary somatosensory (SI_{contra}), contralateral secondary somatosensory (SII_{contra}), and ipsilateral secondary somatosensory cortex activity (SII_{ipsi}). And finally, an auditory dataset (Fig. 9) provides a simple example of initial synchronous, bilateral activity in auditory cortex. This set also includes asynchronous activation of the temporo-parietal junction and cingulate cortex (4 cortical sources).

Empirical Data

As mentioned previously, visual, somatosensory and auditory data have already been acquired from 5 participants. Details regarding these data are described below.

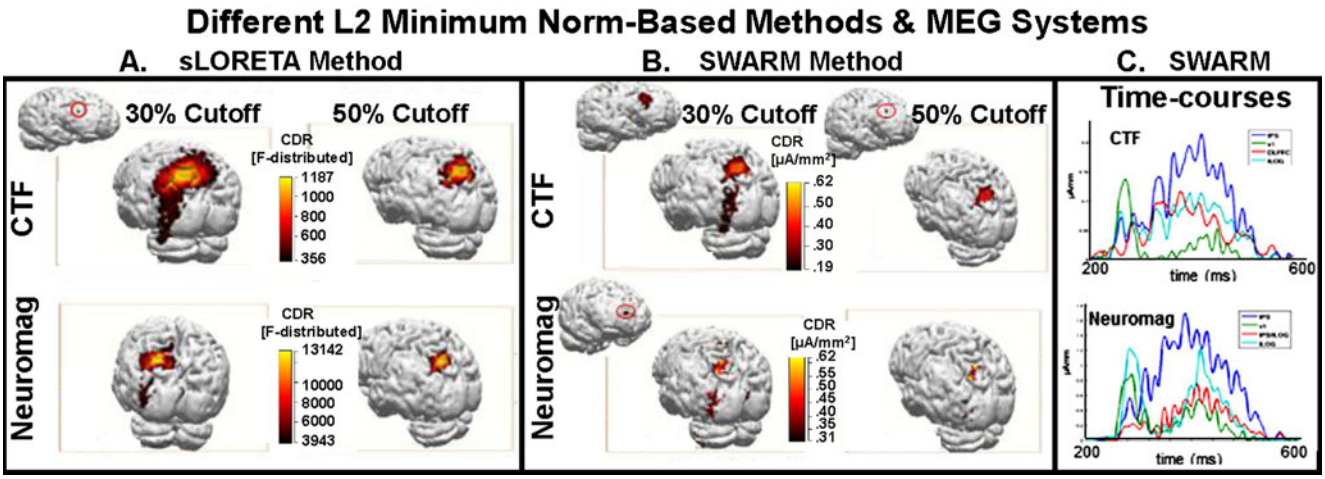

Fig. 7 (**A**) sLORETA results using Curry at two different cutoff values (30% and 50%) for the same active cortical areas mixed with spontaneous noise files from the CTF and Neuromag systems. (**B**) SWARM results using Curry at two cutoff values for the same active cortical areas and noise files used in (**A**). (**C**) Time-course reconstructions from SWARM using simulated datasets in (**B**) (both CTF and Neuromag)

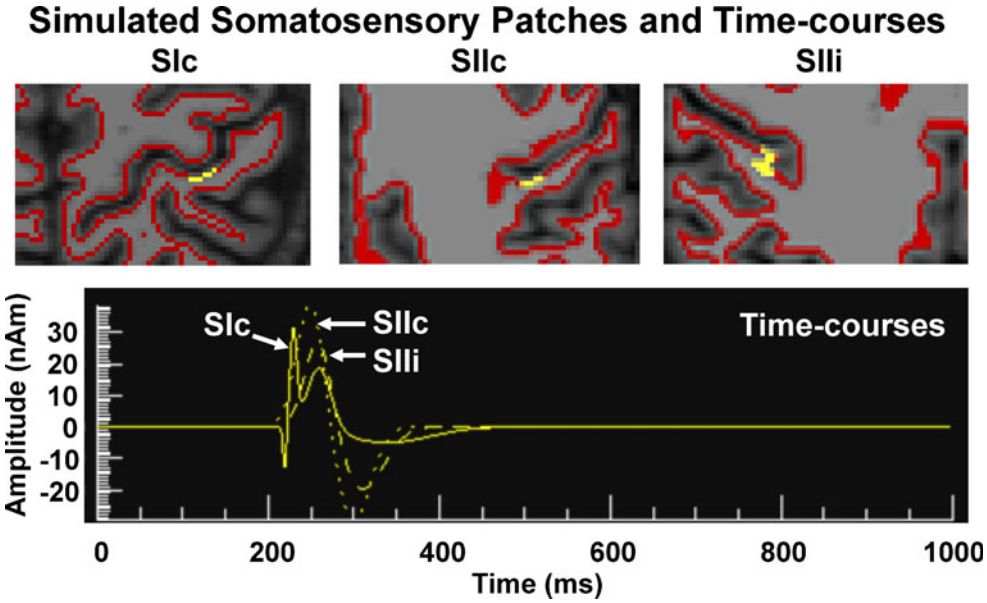

Fig. 8 Primary somatosensory (SIc), contra- and ipsi-lateral secondary somatosensory cortices (SIIc and SIIi) were activated in this example

Visual Study Small visual patterns of two sizes (1.0° and 5.0° of visual angle) were presented at 3.8° eccentricity in the left and right visual fields. The small stimulus was designed to activate ~4 mm^2 of tissue in primary visual cortex (at 3.8° eccentricity) according to the cortical magnification factors presented in Rovamo and Virsu (1979) while the large stimulus was designed to activate ~20 mm^2 of cortex (focal vs. extended sources). The background matched the mean luminance of the bullseye patterns. Participants passively viewed a small fixation point at the center of the screen while the stimuli were randomly presented to the left and right visual fields for a duration of 500 ms and at a rate of 800–1,300 ms (slightly randomized to avoid expectation). Two hundred individual responses for each of two stimulus conditions were averaged together. Visual stimuli were projected onto a backprojection screen using a DLP projector (Projection Design FX1+) outside the magnetically shielded room. The same projector and notebook computer were flown to each site. Stimulus sequences were generated using Presentation software (Neurobehavioral Systems, http://www.neurobs.com/). Eccentricities and visual angle subtended by the stimuli were kept constant across sites by adjusting the stimulus size based on the path lengths measured at each site.

Somatosensory Study An S88 dual channel stimulator with PSISU7 optical stimulus isolation units (Grass Instruments, West Warwick, RI, USA) was used for the somatosensory study. Electrical stimuli were delivered to the median nerve and to the index finger of the right and left hands with an ISI varying between 1.5 and 2 s. The intensity of median nerve stimulation was adjusted to produce a mild thumb

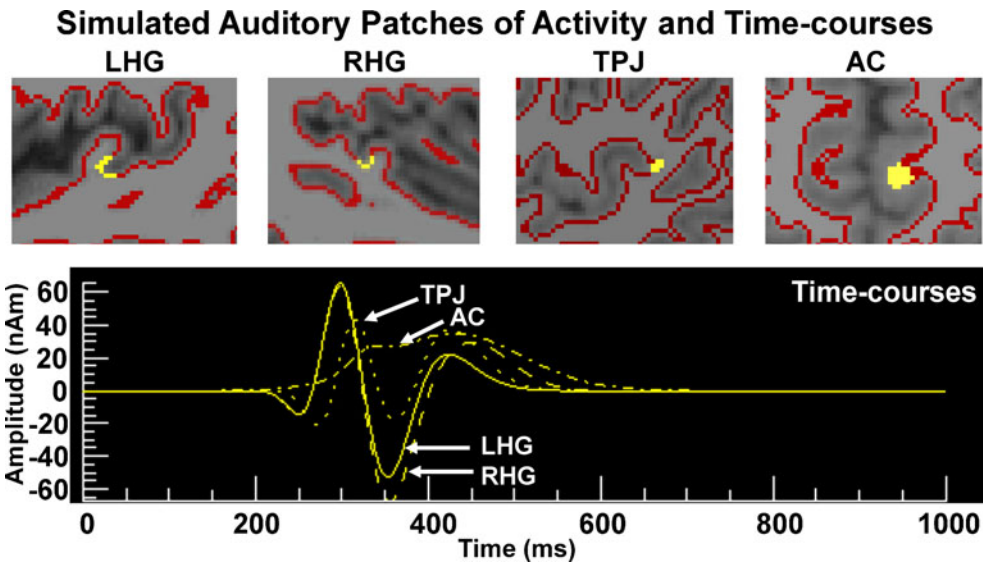

Fig. 9 Simulated auditory data based on 4 regions of activation (Left and right Heschl's gyrus or LHG and RHG; temporo-parietal junction or TPJ; and anterior cingulate or AC)

twitch and the intensity was kept the same for index fingers and median nerves. Initial analyses of these data were presented by Weisend et al. (2007).

Auditory Study In this empirical study, three pure tones of different frequencies (500 Hz, 2,000 Hz, and 4,000 Hz) were presented to obtain a tonotopic map. In addition white noise was also presented intermixed with the tones (focal vs. extended source conditions). White noise contains spectral energy over a wide frequency range in contrast to pure tones, and thus increases the size of the activated cortical patch (Pickles 1988). The cochlea is organized tonotopically and this organization is propagated to primary auditory cortex, where low frequencies are represented rostrally and high frequencies caudally (Schwartz 1986). White noise should stimulate extended tissue covering a range of frequencies. The tones and white noise (200 trials for each stimulus) were randomly presented at an average inter-stimulus interval of 1,000 ms. Auditory stimuli were generated using Presentation software and were presented via a Creative Labs Soundblaster audio card. The sound was delivered to the subject's ear canal using sound transducers connected with plastic tubing to ergonomically designed earplugs. A dB attenuator was used to adjust the intensity of the tones.

Discussion

One goal of this effort is to offer developers of MEG methods, and hopefully EEG methods in the future, an opportunity to directly compare results from their analysis routines with others by using this extensive realistic simulated and empirical testbed of data established for the purpose of quantifying strengths and limitations of each method (standardization). This will aid in the refinement and further development of algorithms. Second, we are all aware that some analysis procedures are better-suited for certain types of studies while other analysis procedures are better-suited for other studies. The extensive testbed of realistic simulated data provided at the web portal (http://cobre.mrn.org/megsim/) includes sample datasets emulating sensory through working memory-related processes across visual, auditory, and somatosensory modalities. Users of MEG analysis procedures should be able to make informed decisions as to which analysis tools are best-suited for their data by working with these datasets. The direct comparison of different analysis techniques is necessary for moving the MEG (and EEG) field forward in the neuroimaging arena.

The creation of single-trial simulated datasets permit a wider variety of MEG analysis tools to be compared. Construction of single trials that mimic the differences between epochs of real data allow the use of analysis techniques such as ICA to be used in conjunction with various source modeling techniques to identify functional networks. These results can then be compared with traditional source analysis conducted on averaged data. With the addition of oscillations to the simulated datasets, analyses of the accuracy of functional connectivity measures between various brain areas can also be investigated. This is important since it is incomplete to know, for example, that certain brain locations are active without information about which areas onset first, their durations, and whether cross-frequency oscillatory activity is evident across multiple disparate brain regions or not. Furthermore, the simulated datasets described here are available in a variety of file formats, including netCDF, Neuromag .fif, CTF .ds, and Curry (Compumedics, Neuroscan). Hopefully, the creation of these new datasets and formats, including novel single trial simulations, will foster algorithm performance comparisons and facilitate cross-site collaborations. All datasets and single trials discussed herein are currently available at the web portal (http://cobre.mrn.org/megsim/).

Information Sharing Statement

All data necessary to reproduce our analyses are located on the web portal available to all interested parties (http://cobre.mrn.org/megsim/). MRI (MPRAGE), segmented MRI, cortical surfaces, BEM surfaces and ground truth source distributions are available. Where appropriate, IDL utilities will be supplied to write data to text formats. A free MATLAB utility exists that permits reading netCDF format into MATLAB. The web portal has links to download MRIVIEW and MEGAN as well as functions that import data from netMEG files into C or IDL so that additional simulations can be constructed by others.

Acknowledgment This work was funded by NIH grants R21MH080141-02, 1P20 RR021938-03, and R01AG029495-03. It was also supported in part by the Department of Energy under Award Number DE-FG02-99ER62764 to the Mind Research Network. We thank M. Weisend, S. Ahlfors, M. Hämäläinen, J. Mosher, A. Leuthold, and A. Georgopoulos for their help when the initial partnership between institutions was established which permitted the acquisition of these data. The content of this study is solely the responsibility of the authors and does not necessarily represent the official views of the National Institutes of Health. Furthermore, the authors declare that they have no conflict of interest.

References

Ahlfors, S. P., Han, J., Lin, F. H., Witzel, T., Belliveau, J. W., Hämäläinen, M. S., et al. (2010). Cancellation of EEG and MEG signals generated by extended and distributed sources. *Human Brain Mapping, 31*, 140–149.

Aine, C., Adair, J., Knoefel, J., Hudson, D., Qualls, C., Kovacevic, S., et al. (2005). Temporal dynamics of age-related differences in auditory incidental verbal learning. *Cognitive Brain Research, 24*, 1–18.

Aine, C., Huang, M., Stephen, J., & Christner, R. (2000). Multistart algorithms for MEG empirical data analysis reliably characterize locations and time courses of multiple sources. *NeuroImage, 12*, 159–172.

Aine, C. J., Bryant, J. E., Knoefel, J. E., Adair, J. C., Hart, B., Donahue, C. H., et al. (2010). Different strategies for auditory word recognition in healthy versus normal aging. *NeuroImage, 49*, 3319–3330.

Aine, C. J., Stephen, J. M., Christner, R., Hudson, D., & Best, E. (2003). Task relevance enhances early transient and late slow-wave activity of distributed cortical sources. *Journal of Computational Neuroscience, 15*, 203–221.

Aine, C. J., Supek, S., George, J. S., Ranken, D., Lewine, J., Sanders, J., et al. (1996). Retinotopic organization of human visual cortex: departures from the classical model. *Cerebral Cortex, 6*, 354–361.

Aine, C. J., Woodruff, C. C., Knoefel, J. E., Adair, J. C., Hudson, D., Qualls, C., et al. (2006). Aging: Compensation or maturation? *NeuroImage, 32*, 1891–1904.

Amunts, K., Malikovic, A., Mohlberg, H., Schormann, T., & Zilles, K. (2000). Brodmann's areas 17 and 18 brought into stereotaxic space-where and how variable? *NeuroImage, 11*, 66–84.

Baillet, S., Mosher, J., & Leahy, R. (2001). Electromagnetic brain mapping. IEEE Signal Processing Magazine: 14–30.

Bisley, J. W., Krishna, B. S., & Goldberg, M. E. (2004). A rapid and precise on-response in posterior parietal cortex. *Journal of Neuroscience, 24*, 1833–1838.

Brookes, M. J., Stevenson, C. M., Barnes, G. R., Hillebrand, A., Simpson, M. I., Francis, S. T., et al. (2007). Beamformer reconstruction of correlated sources using a modified source model. *NeuroImage, 34*, 1454–1465.

Canolty, R. T., Edwards, E., Dalal, S. S., Soltani, M., Nagarajan, S. S., Kirsch, H. E., et al. (2006). High gamma power is phase-locked to theta oscillations in human neocortex. *Science, 313*, 1626–1628.

Cauller, L. J. (1998). Backward Cortical Projections to primary somatosensory cortex in rats extend long horizontal axons in layer I. *The Journal of Comparative Neurology, 390*, 297–310.

Dalal, S. S., Sekihara, K., & Nagarajan, S. S. (2006). Modified beamformers for coherent source region suppression. *IEEE Transactions on Biomedical Engineering, 53*, 1357–1363.

Dale, A. M., Liu, A. K., Fischl, B. R., Buckner, R. L., Belliveau, J. W., Lewine, J. D., et al. (2000). Dynamic statistical parametric mapping: combining fMRI and MEG for high-resolution imaging of cortical activity. *Neuron, 26*, 55–67.

Dale, A. M., & Sereno, M. I. (1993). Improved localization of cortical activity by combining EEG and MEG with MRI cortical surface reconstruction: A linear approach. *Journal of Cognitive Neuroscience, 5*, 162–176.

David, O., Garnero, L., Cosmelli, D., & Varela, F. J. (2002). Estimation of neural dynamics from MEG/EEG cortical current density maps: application to the reconstruction of large-scale cortical synchrony. *IEEE BME, 49*, 975–987.

de Lange, F. P., Jensen, O., Bauer, M., & Toni, I. (2008). Interactions between posterior gamma and frontal alpha/beta oscillations during imagined actions. *Frontiers in Human Neuroscience, 2*, 7.

Diwakar, M., Huang, M. X., Srinivasan, R., Harrington, D. L., Robb, A., Angeles, A., et al. (2011). Dual-Core Beamformer for obtaining highly correlated neuronal networks in MEG. *NeuroImage, 54*, 253–263.

Engel, A. K., Fries, P., & Singer, W. (2001). Dynamic predictions: oscillations and synchrony in top-down processing. *Nature Reviews Neuroscience, 2*, 704–716.

Ermer, J. J., Mosher, J. C., Baillet, S., & Leah, R. M. (2001). Rapidly recomputable EEG forward models for realistic head shapes. *Physics in Medicine and Biology, 46*, 1265–1281.

Ermer, J. J., Mosher, J. C., Huang, M., & Leahy, R. M. (2000). Paired MEG data set source localization using recursively applied and projected (RAP) MUSIC. *IEEE Transactions on Biomedical Engineering, 47*, 1248–1260.

Fuchs, M., Wagner, M., Kohler, T., & Wischmann, H. A. (1999). Linear and nonlinear current density reconstructions. *Journal of Clinical Neurophysiology, 16*, 267–295.

Golubic, S. J., Susac, A., Grilj, V., Ranken, D., Huonker, R., Haueisen, J., et al. (2011). Size matters: MEG empirical and simulation study on source localization of the earliest visual activity in the occipital cortex. *Medical & Biological Engineering & Computing, 49*, 545–554.

Grave de Peralta-Menendez, R., & Gonzalez-Andino, S. L. (1998). A critical analysis of linear inverse solutions to the neuroelectromagnetic inverse problem. *IEEE Transactions on Biomedical Engineering, 45*, 440–448.

Gray, C. M., Konig, P., Engel, A. K., & Singer, W. (1989). Oscillatory responses in cat visual cortex exhibit inter-columnar synchronization which reflects global stimulus properties. *Nature, 338*, 334–337.

Greenblatt, R. E., Ossadtchi, A., & Pflieger, M. E. (2005). Local linear estimators for the bioelectromagnetic inverse problem. *IEEE Transactions on Signal Processing, 53*, 3403–3412.

Hämäläinen, M., Hari, R., Ilmoniemi, R., Knuutila, J., & Lounasmaa, O. (1993). Magnetoencephalography? Theory, instrumentation, and applications to noninvasive studies of the working human brain. *Reviews of Modern Physics, 65*, 413–497.

Hämäläinen, M. S., & Ilmoniemi, R. J. (1994). Interpreting magnetic fields of the brain: minimum norm estimates. *Medical & Biological Engineering & Computing, 32*, 35–42.

Harrison, R., Aine, C., Chen, H.-W., & Flynn, E. (1996). Comparison of minimization methods for spatio-temporal electromagnetic source localization using temporal constraints. *NeuroImage, 3*, S64.

Hillebrand, A., & Barnes, G. R. (2002). A quantitative assessment of the sensitivity of whole-head MEG to activity in the adult human cortex. *NeuroImage, 16*, 638–650.

Huang, M., Aine, C. J., Supek, S., Best, E., Ranken, D., & Flynn, E. R. (1998). Multi-start downhill simplex method for spatio-temporal source localization in magnetoencephalography. *Electroencephalography and Clinical Neurophysiology, 108*, 32–44.

Huang, M. X., Dale, A. M., Song, T., Halgren, E., Harrington, D. L., Podgorny, I., et al. (2006). Vector-based spatial-temporal minimum L1-norm solution for MEG. *NeuroImage, 31*, 1025–1037.

Huang, M. X., Mosher, J. C., & Leahy, R. M. (1999). A sensor-weighted overlapping-sphere head model and exhaustive head model comparison for MEG. *Physics in Medicine and Biology, 44*, 423–440.

Hui, H. B., & Leahy, R. M. (2006). Linearly constrained MEG beamformers for MVAR modeling of cortical interactions, 3rd IEEE International Symposium on Biomedical Imaging: Macro to Nano. 237–240.

Hui, H. B., Pantazis, D., Bressler, S. L., & Leahy, R. M. (2010). Identifying true cortical interactions in MEG using the nulling beamformer. *NeuroImage, 49*, 3161–3174.

Ioannides, A. A., Bolton, J. P., & Clarke, C. J. S. (1990). Continous probabilistic solutions to the biomagnetic inverse problem. *Inverse Problems, 6*, 523–542.

Ioannides, A. A., Fenwick, P. B., Lumsden, J., Liu, M. J., Bamidis, P. D., Squires, K. C., et al. (1994). Activation sequence of discrete brain areas during cognitive processes: results from magnetic field tomography. *Electroencephalography and Clinical Neurophysiology, 91*, 399–402.

Jensen, O., & Lisman, J. E. (1998). An oscillatory short-term memory buffer model can account for data on the Sternberg task. *Journal of Neuroscience, 18*, 10688–10699.

Jun, S. C., George, J. S., Paré-Blagoev, J., Plis, S. M., Ranken, D. M., Schmidt, D. M., et al. (2005). Spatiotemporal Bayesian inference dipole analysis for MEG neuroimaging data. *NeuroImage, 28*, 84–98.

Kovacevic, S., Qualls, C., Adair, J., Hudson, D., Woodruff, C., Knoefel, J., et al. (2005). Age-related effects on superior temmporal gyrus activity during an oddball task. *Neuroreport, 16*, 1075–1079.

Lamme, V. A., & Roelfsema, P. R. (2000). The distinct modes of vision offered by feedforward and recurrent processing. *Trends in Neurosciences, 23*, 571–579.

Lampl, I., Reichova, I., & Ferster, D. (1999). Synchronous membrane potential fluctuations in neurons of the cat visual cortex. *Neuron, 22*, 361–374.

Liljestrom, M., Kujala, J., Jensen, O., & Salmelin, R. (2005). Neuromagnetic localization of rhythmic activity in the human brain: a comparison of three methods. *NeuroImage, 25*, 734–745.

Lin, F. H., Witzel, T., Ahlfors, S. P., Stufflebeam, S. M., Belliveau, J. W., & Hämäläinen, M. S. (2006). Assessing and improving the spatial accuracy in MEG source localization by depth-weighted minimum-norm estimates. *NeuroImage, 31*, 160–171.

Liu, A. K., Belliveau, J. W., & Dale, A. M. (1998). Spatiotemporal imaging of human brain activity using functional MRI constrained magnetoencephalography data: Monte Carlo simulations. *Proceedings of the National Academy of Sciences of the United States of America, 95*, 8945–8950.

Luck, S. J. (2005). *An introduction to the event-related potential technique*. MIT Press.

Mattout, J., Phillips, C., Penny, W. D., Rugg, M. D., & Friston, K. J. (2006). MEG source localization under multiple constraints: an extended Bayesian framework. *NeuroImage, 30*, 753–767.

Mehta, A. D., Ulbert, I., & Schroeder, C. E. (2000). Intermodal selective attention in monkeys. II: physiological mechanisms of modulation. *Cerebral Cortex, 10*, 359–370.

Michel, C. M., Murray, M. M., Lantz, G., Gonzalez, S., Spinelli, L., & Grave de Peralta, R. (2004). EEG source imaging. *Clinical Neurophysiology, 115*, 2195–2222.

Moiseev, A., Gaspar, J. M., Schneider, J. A., & Herdman, A. T. (2011). Application of multi-source minimum variance beamformers for reconstruction of correlated neural activity. *NeuroImage, 58*, 481–489.

Mosher, J. C., Lewis, P. S., & Leahy, R. M. (1992). Multiple dipole modeling and localization from spatio-temporal MEG data. *IEEE Transactions on Biomedical Engineering, 39*, 541–557.

Nelder, J., & Mead, R. (1965). A simplex method for function minimization. *The Computer Journal, 7*, 308–313.

Nyberg, L., Marklund, P., Persson, J., Cabeza, R., Forkstam, C., Petersson, K. M., et al. (2003). Common prefrontal activations during working memory, episodic memory, and semantic memory. *Neuropsychologia, 41*, 371–377.

Osipova, D., Hermes, D., & Jensen, O. (2008). Gamma power is phase-locked to posterior alpha activity. *PLoS One, 3*, e3990.

Pascual-Marqui, R. D. (2002). Standardized low-resolution brain electromagnetic tomography (sLORETA): technical details. *Methods and Findings in Experimental and Clinical Pharmacology, 24* (Suppl D), 5–12.

Pascual-Marqui, R. D., Lehmann, D., Koenig, T., Kochi, K., Merlo, M. C., Hell, D., et al. (1999). Low resolution brain electromagnetic tomography (LORETA) functional imaging in acute, neuroleptic-naive, first-episode, productive schizophrenia. *Psychiatry Research, 90*, 169–179.

Pascual-Marqui, R. D., Michel, C. M., & Lehmann, D. (1994). Low resolution electromagnetic tomography: a new method for localizing electrical activity in the brain. *International Journal of Psychophysiology, 18*, 49–65.

Pickles, J. O. (1988). *An introduction to the physiology of hearing* (2nd ed.). San Diego: Academic.

Portin, K., Vanni, S., Virsu, V., & Hari, R. (1999). Stronger occipital cortical activation to lower than upper visual field stimuli. Neuromagnetic recordings. *Experimental Brain Research, 124*, 287–294.

Ranken, D., Best, E., Schmidt, D. M., George, J. S., Wood, C. C., & Huang, M. (2002). MEG/EEG forward and inverse modeling using MRIVIEW. In H. Nowak, J. Jaueisen, F. Giebler and R. Huonker (Eds.), *Proceedings of the 13th international conference on biomagnetism*, pp. 785–787.

Ranken, D., & George, J. S. (1993). MRIVIEW: An interactive computational tool for investigation of brain structure and function. In *Proceedings of the IEEE visualization '93*. IEEE Computer Society Press, pp. 324–331.

Ranken, D. M., Stephen, J. M., & George, J. S. (2004). MUSIC seeded multi-dipole MEG modeling using the Constrained Start Spatio-Temporal modeling procedure. *Neurology and Clinical Neurophysiology, 2004*, 80.

Rovamo, J., & Virsu, V. (1979). An estimation and application of the human cortical magnification factor. *Experimental Brain Research, 37*, 495–510.

Sarvas, J. (1987). Basic mathematical and electromagnetic concepts of the biomagnetic inverse problem. *Physics in Medicine and Biology, 32*, 11–22.

Scherg, M., & Von Cramon, D. (1986). Evoked dipole source potentials of the human auditory cortex. *Electroencephalography and Clinical Neurophysiology, 65*, 344–360.

Schmidt, D. M., George, J. S., & Wood, C. C. (1999). Bayesian inference applied to the electromagnetic inverse problem. *Human Brain Mapping, 7*, 195–212.

Schwartz, A. M. (1986). Auditory nerve and spiral ganglion cells: Morphology and organization. In R. A. Altschuler, R. P. Bobbin, & D. W. Hoffman (Eds.), *Neurobiology of hearing: The cochlea* (pp. 271–282). New York: Raven.

Sekihara, K., Nagarajan, S. S., Poeppel, D., Marantz, A., & Miyashita, Y. (2001). Reconstructing spatio-temporal activities of neural sources using an MEG vector beamformer technique. *IEEE Transactions on Biomedical Engineering, 48*, 760–771.

Singer, W. (1999). Neuronal synchrony: a versatile code for the definition of relations? *Neuron, 24*(49–65), 111–125.

Stephen, J. M., Aine, C. J., Christner, R. F., Ranken, D., Huang, M., & Best, E. (2002). Central versus peripheral visual field stimulation results in timing differences in dorsal stream sources as measured with MEG. *Vision Research, 42*, 3059–3074.

Stephen, J. M., Aine, C. J., Ranken, D., Hudson, D., & Shih, J. J. (2003a). Multidipole analysis of simulated epileptic spikes with real background activity. *Journal of Clinical Neurophysiology, 20*, 1–16.

Stephen, J. M., Davis, L. E., Aine, C. J., Ranken, D., Herman, M., Hudson, D., et al. (2003b). Investigation of the normal proximal somatomotor system using magnetoencephalography. *Clinical Neurophysiology, 114*, 1781–1792.

Stephen, J. M., Ranken, D., Best, E., Adair, J., Knoefel, J., Kovacevic, S., et al. (2006). Aging changes and gender differences in response to median nerve stimulation measured with MEG. *Clinical Neurophysiology, 117*, 131–143.

Stephen, J. M., Ranken, D. M., Aine, C. J., Weisend, M. P., & Shih, J. J. (2005). Differentiability of simulated MEG hippocampal, medial temporal and neocortical temporal epileptic spike activity. *Journal of Clinical Neurophysiology, 22*, 388–401.

Sun, M. (1997). An efficient algorithm for computing multishell spherical volume conductor models in EEG dipole source localization. *IEEE BME, 44*, 1243–1252.

Supek, S., & Aine, C. (1997). Spatio-temporal modeling of neuromagnetic data: I. Multisource location vs. timecourse estimation accuracy. *Human Brain Mapping, 5*, 139–153.

Susac, A., Ilmoniemi, R. J., Pihko, E., Ranken, D., & Supek, S. (2010). Early cortical responses are sensitive to changes in face stimuli. *Brain Research, 1346*, 155–164.

Susac, A., Ilmoniemi, R. J., Ranken, D., & Supek, S. (2011). Face activated neurodynamic cortical networks. *Medical & Biological Engineering & Computing, 49*, 531–543.

Uutela, K., Hämäläinen, M., & Somersalo, E. (1999). Visualization of magnetoencephalographic data using minimum current estimates. *NeuroImage, 10*, 173–180.

Van Veen, B. D., van Drongelen, W., Yuchtman, M., & Suzuki, A. (1997). Localization of brain electrical activity via linearly constrained minimum variance spatial filtering. *IEEE Transactions on Biomedical Engineering, 44*, 867–880.

Vanni, S., Dojat, M., Warnking, J., Delon-Martin, C., Segebarth, C., & Bullier, J. (2004). Timing of interactions across the visual field in the human cortex. *NeuroImage, 21*, 818–828.

von Stein, A., Chiang, C., & Konig, P. (2000). Top-down processing mediated by interareal synchronization. *Proceedings of the National Academy of Sciences of the United States of America, 97*, 14748–14753.

Vrba, J., & Robinson, S. E. (2000). Linearly constrained minimum variance beamformers, synthetic aperture magnetometry, and MUSIC in MEG applications. *IEEE Conference Record of the 34th Asilomar Conference on Signals, Systems and Computers*, Vol. 1, 313–317.

Wagner, M., Fuchs, M., & Kastner, J. (2004). Evaluation of sLORETA in the presence of noise and multiple sources. *Brain Topography, 16*, 277–280.

Wagner, M., Fuchs, M., & Kastner, J. (2007) *SWARM: sLORETA-weighted accurate minimum-norm inverse solutions*. Proceedings of the 15th International Conference on Biomagnetism. Vancouver, BC Canada, Elsevier ICS 1300.

Wagner, M., Fuchs, M., & Kastner, J. (2008). sLORETA, eLORETA, and SWARM in the presence of noise and multiple sources. In R. Kakigi, K. Yokosawa, S. Kuriki (Eds.), *Biomagnetism: Interdisciplinary research and exploration*. Hokkaido University Press, pp. 74–76.

Wang, J. Z., Williamson, S. J., & Kaufman, L. (1992). Magnetic source images determined by a lead-field analysis: the unique minimum-norm least-squares estimation. *IEEE Transactions on Biomedical Engineering, 39*, 665–675.

Weisend, M., Hanlon, F. M., Montano, R., Ahlfors, S., Leuthold, A. C., Pantazis, D., et al. (2007). Paving the way for cross-site pooling of magnetoencephalography (MEG) data. *International Congress Series, 1300*, 615–618.

Wischmann, H. A., Fuchs, M., Wagner, A. D., & Doessel, O. (1995). Current density imaging: A time series reconstruction implementing a "best fixed distributions" constraint. In C. Baumgartner, L. Deecke, G. Stroink, & S. J. Williamson (Eds.), *Biomagnetism: Fundamental research and clinical applications* (pp. 427–432). Amsterdam: Ios Press.

Wipf, D. P., Owen, J. P., Attias, H. T., Sekihara, K., & Nagarajan, S. S. (2010). Robust Bayesian estimation of the location, orientation, and time course of multiple correlated neural sources using MEG. *NeuroImage, 49*, 641–655.